Injectable and NIR-Responsive CDN-POM Hydrogels for Combined Non-Inflammatory Photo-immunotherapy

Hailong Jiang

1379170113@qq.com

Sun Yat-sen University

Die Liu

Sun Yat-sen University

Jianing Wang

Sun Yat-sen University

Jingchao Li

Zhejiang University School of Medicine

Xinrui Pang

Sun Yat-sen University

Ke Zhang

Sun Yat-sen University

Hong Shan

Sun Yat-sen University

Research Article

Keywords: breast tumor, photothermal, ROS-scavenging, Cyclic dinucleotides, combination therapy

Posted Date: April 17th, 2024

DOI: https://doi.org/10.21203/rs.3.rs-4240392/v1

Additional Declarations: No competing interests reported.

Abstract

Similar to clinically applied thermal ablation techniques, the cellular necrosis that occurs during photothermal tumor therapy (PTT) can induce inflammatory response, severely compromising the therapeutic efficacy and clinical translation of PTT. Inspired by the remarkable ROS-scavenging activity and high photothermal efficiency of molybdenum-based polyoxometalate (POM) and immunostimulatory effect of Cyclic dinucleotides (CDNs), a NIR-responsive and injectable DNA-mediated hybrid hydrogel (CDN-POM) is developed. The hydrogels have superior photothermal efficiency (43.41%) to POM, impressive anti-inflammatory capability and prolonged intratumoral CDN-releasing behavior, thus enabling synergistic anti-tumor therapeutic outcomes. Meanwhile, local treatment induced by CDN-POM hydrogels displays minimal side effects on normal tissue. Taking advantage of the high phototherapeutic effect, ROS-scavenging activity and sustained CDN release of CDN-POM hydrogels, a novel combined approach that integrates the photothermal and immunotherapy of breast tumor is successfully pioneered.

Introduction

Breast tumor, characterized by high morbidity and mortality, is the primary factor threatening worldwide women's health [1–3]. Despite the great efforts made in the last decades, surgical excision remains the main treatment because of its simplicity of operation[4]. However, it is still challenging to completely eliminate solid tumors, leading to inevitable tumor recurrence. Furthermore, surgical excision and postoperative medications could cause primary damage to normal tissues[5–7]and organs[8, 9]. Consequently, effective synergistic strategies should be elaborated to improve the therapeutic efficacy and alleviate the side effects of breast tumor treatment[10].

Photothermal therapy (PTT) has received increasing attention in breast tumor therapy due to its advantages of minor damage to non-target tissues and low invasiveness[11, 12]. However, although PTT could achieve rapid and effective ablation of tumors; the released intracellular components would trigger adverse inflammatory responses and hamper the therapeutic efficacy[13]. In addition to pro-inflammatory cytokines and proteins, the accumulation of highly reactive oxygen species (ROS) also plays a crucial role in stimulating tumor recurrence and damaging peripheral normal cells[14–16]. Molybdenum (Mo)-based polyoxometalate (POM) clusters have emerged as promising mediators of PTT due to their small size, efficient light-to-heat conversion, good biosafety, remarkable ROS-scavenging activity and anti-inflammatory effects[17–19]. Unfortunately, conventional intravenous administration of POM would decrease their tumor accumulation, thereby weakening the POM-induced photothermal effect at the tumor site and metabolizing more rapidly[20–22]. Therefore, it is of great importance to develop novel photothermal materials for tumor-targeting treatment with ideal safety to peripheral normal cells.

Cancer immunotherapy has emerged as an revolutionary therapeutic approach to generate specific and durable anti-tumor responses by harnessing the natural immune system of the host[23, 24]. The

stimulator of interferon genes (STING) is a type of intracellular signaling receptor that activates innate immune cells downstream[25–27]. Cyclic dinucleotides (CDN) are specially designed and synthesized as non-nucleotide STING-activating agonists[28–30]. Tumor-bearing CDN is a promising candidate in clinical antitumor trials (NCT02675439), and it has demonstrated efficacy in tumor-bearing mice in promoting specific inhibition of various tumors [31–33]. Nevertheless, the effectiveness of agonists is significantly reduced due to metabolic instability and rapid clearance from the body after systemic administration [31, 34, 35]. Therefore, novel strategies to improve the efficacy of CDN in tumor treatment are urgently needed.

In this study, we developed a NIR-responsive and injectable hybrid hydrogel (denoted as CDN-POM), which could reduce PTT-induced inflammation for photothermally ablating tumors and releasing CDN to activate innate antitumor immunity (Fig. 1)[36]. Compared to POM, CDN-POM hydrogels exhibited superior photothermal conversion capability of rapid heating under the same near-infrared irradiation. Apart from this, the biocompatible CDN-POM hydrogels were capable of showing remarkable ROS-scavenging activity to suppress PTT-induced inflammatory responses. Meanwhile, the CDN-POM hydrogels enabled continuable release of CDN for a prolonged time, resulting in a rapid, sustained and effective activation of the STING pathway. Thus, CDN-POM hydrogels that integrate the advantages of higher photothermal effect, excellent ROS-scavenging ability and effectively sustained activation of STING pathway could become a prospective medical composite for combined cancer therapy.

Preparation and characterization of CDN-POM hybrid hydrogels

As illustrated in Fig. 2A, the injectable CDN-POM hybrid hydrogels were successfully constructed *via* a DNA mediated self-assembly method. Firstly, POM was prepared by a redox method and then used as the cross linker to form hybrids with CDN, salmon sperm DNA (smDNA, 2000 bp) and polylysines (PLL,1000 bp). The transmission emission microscopy (TEM) images showed that POM exhibited an average diameter of 1–2 nm. Ultimately, the CDN-POM hydrogel was formed by electrostatic complexation of POM and smDNA and with cationic PLL (Fig. 2A). The scanning electron microscopy showed that the hydrogels proved a porous interconnected structure by adding CDN and PLL. (Fig. 2B). This suggested that PLL could electrostatically attract POM and CDN to form a compact and confined network. Then we conducted *in vivo* photoacoustic imaging experiments of POM and CDN-POM hybrid hydrogels in 4T1 tumor-bearing mice. Before the injection, relatively weak photoacoustic signals of tumor tissues were detected due to the background signal produced by intrinsic hemoglobin and melanin. Within 8 h after the injection of POM, the PA signal gradually disappeared, indicating that POM had been rapidly excreted from the tumor tissue (SI Fig. 1). However, at 24 h post-injection, the PA signal of the CDN-POM hybrid hydrogel was still evident. PA images showed that CDN-POM hybrid hydrogel could prolong tumor retention for the long-acting release of CDN. The rheometer results indicated that the CDN-POM hydrogel had a low viscosity (Fig. 2C), making it possible to be injected *via* syringe (Fig. 2D). In the measured frequency range (0.1–100 Hz), the storage modulus (G') was larger compared

to the loss modulus (G"), which proved the typical viscoelastic property of CDN-POM hydrogels. (Figure.2D).

The photothermal performance of the CDN–POM hydrogels

Subsequently, we compared the photothermal performance of POM and CDN–POM hydrogels. First, various CDN–POM hydrogels with different concentrations of POM were fabricated. The CDN–POM hydrogel (0.2 wt% POM) exhibited a fast-heating rate, and it could reach 54°C under 808 nm laser irradiation (1 W cm^{-2}) for 30 s. After irradiation for 3 min, the temperature of hydrogel was up to 89°C. In contrast, the POM with the same concentration exhibited less photothermal efficiency (Fig. 3A), which was confirmed by the thermal images of samples with different concentrations (Fig. 3B). In the CDN–POM hydrogels, the photothermal conversion efficiency (η) was calculated to be 43.4%, which was much higher than that of the pristine POM (32.3%) (Fig. 3D and SI Fig. 3). Those results indicated the confined network formed by the compounding of POM and CDN with PLL played an important role in the extraordinary photothermal effect, which was superior to conventional photothermal systems. Additionally, in the hydrogels, the change of the photothermal effect was negligible after several cycles of laser irradiation, well demonstrating the extraordinary photothermal stability of these hybrid hydrogel materials (Fig. 3C).

Investigation of POM-based photothermal cell-killing ability and ROS scavenging effect.

Inspired by the impressive photothermal conversion ability and negligible cytotoxicity of POM, we therefore evaluated their localized photothermal ablation effect on 4T1 cells under 808 nm laser irradiation (Fig. 4A). No obvious cell necrosis was detected in 4T1 cells when incubated with gradient concentrations of POM for different periods, further indicating the good biocompatibility of POM (Fig. 4A and 4B). The safety of the 808 nm laser irradiation was demonstrated by the fact that no obvious dead cells were observed under the power density of 2.0 W/cm^2 for 5 min without adding POM. After co-incubating 4T1 cells with POM (400 μg/mL, 100 μL) and irradiating the co-incubation sample with 808 nm laser for 5 min, obvious cell necrosis (propidium iodide staining showed red fluorescence) was observed in the area irradiated by NIR light. The area of dead cells could be changed by either the concentration of POM or the power density of NIR laser irradiation.

These results demonstrated the NIR light-induced cell-killing ability of POM. Next, the ROS-scavenging activity of POM in 293T cells was further investigated through ROS threated by using H_2O_2. The intense green fluorescence in 293T cells, resulting from the oxidation of ROS probe (DCFH-DA) by H_2O_2, was gradually weakened by incubating POM with various concentrations (Fig. 4B). The successful elimination of ROS by POM significantly increased cell viability, as confirmed by typical live/dead cell staining (Fig. 4C). Therefore, the above data could demonstrate that the POM has extraordinary ability in NIR photothermal conversion and ROS scavenging.

Investigation of the in vivo anticancer effect of CDN–POM hydrogels

To investigate the anticancer effect *in vivo*, female BALB/c mice bearing 4T1 tumors with a volume of about 100 mm^3 on the dorsum of the right hind leg were used as animal models. Five randomly grouped mice (n = 5) were treated with PBS + NIR laser, POM + NIR laser, CDN–POM hydrogels, free CDN and the CDN–POM hydrogels + NIR laser, injected around the tumors (Fig. 5A). An infrared thermal camera was applied to simultaneously record the real-time temperature changes. Compared to the slight warming (∼1.9°C) of the PBS + NIR laser group, the tumor temperature of the CDN-POM hydrogel reached 58.3°C, compared to 50.6°C of POM, which could normally lead to tumor cell necrosis. No obvious noticeable bodyweight body weight during the treatment course in all groups (SI Fig. 4), indicating that all of the therapeutic agents were non-toxic for 4T1 tumor-bearing mice. After monitoring the tumor volume for 3 weeks, significant tumor inhibition could be observed with the coexistence of the free CDN, POM + NIR and the CDN–POM hydrogel + NIR laser irradiation (Fig. 5B). Under NIR laser irradiation, the group with POM treatment showed similar rapid tumor growth performance compared to the PBS-treated mice, revealing the low toxicity of POM, which was further confirmed by body weight (SI) and pathological features of major organs (Fig. 5D).

Determination of the levels of inflammation-related cytokines

The immunostimulatory activity of the CDN–POM hydrogels in 4T1 tumor-bearing mice was evaluated. In light of the excellent activity of the CDN in stimulating the STING pathway, we further investigated whether the stimulation of the CDN–POM hydrogels could induce DC maturation *in vivo*. The assays focused on the expression of major histocompatibility complex II (MHC- II) and CD11c in BMDCs (splenocytes, flow cytometry). As shown in Fig. 6A, free CDN and CDN–POM hydrogels + NIR significantly upregulated the expression of MHC II and costimulatory markers of CD11c in BMDCs (SI Figure.5). Next, we performed flow analysis to study the expression of $CD4^+$ and $CD8^+$ T cells in the spleen after different treatments. Mice treated with PBS + NIR, POM + NIR, CDN–POM hydrogels induced an average of 4.51% $CD8^+$ T-cells on day 8 (7 days after the injection) (Figure.6B). In contrast, mice treated with the CDN–POM hydrogels + NIR elicited 17.20% $CD8^+$ T-cells, which was 3.81-fold higher than the PBS group ($P < 0.01$), and elicited 13.60% $CD8^+$ T-cells treated with free CDN (SI Figure.6). These experimental results indicated that CDN–POM hydrogels enabled the controlled liberation of CDN, which would eventually facilitate the activation of the STING pathway and increase the tumor infiltration of $CD4^+$ T cells and $CD8^+$ T cells, suggesting the CDN–POM hydrogel is a promising platform to elicit potent T-cell response for efficient tumor immunotherapy.

Immunoregulatory efficacy of CDN–POM hydrogels

Although PTT is effective in inhibiting primary tumors, the adverse release of intracellular constituents caused by high-temperature PTT would induce acute inflammation that may increase the probability of tumor recurrence and metastasis. Inspired by the considerable ROS scavenging activities of POM *in vitro*, the inflammatory-related cytokine levels in tumors of mice after various treatments were

determined. As shown in Fig. 7Aand 7B, due to the ROS-eliminating function of POM, no significant increase of inflammatory-related cytokine levels could be observed in POM + NIR group and the CDN–POM hydrogel + NIR group compared with the PBS + NIR gruop. Therefore, these findings proved that the CDN-POM hydrogels could be used for photothermal cancer treatment under NIR laser irradiation with minimal adverse inflammatory responses.

Conclusion

In this work, an unprecedented method based on NIR-responsive and injectable CDN-POM hybrid hydrogel with remarkable PTT capacity and innate antitumor immunity-activating performance has been developed for combined tumor photo-immunotherapy. In contrast to POM, the CDN-POM hydrogels have outstanding biocompatibility, superior photothermal efficiency (43.4%) and thermal stability. In addition, CDN-POM hydrogel also has excellent ROS scavenging ability to overpower the inflammatory response induced by the conventional PTT. Meanwhile, the CDN released by CDN-POM hydrogels can create a local environment with a high concentration of CDN to activate immune response *in vivo*, including massive recruitment of $CD8^+$ cells and CD11c in MDSC. As a proof-of-concept study, our work favors the combination of non-inflammatory PTT with immunotherapy based on POM-CDN hydrogels for efficient breast cancer therapy.

Methods

Preparation of POM. POM was synthesized by a one-pot method. Briefly, 2.50 g Molybdic acid ammonium salt ($NH_4Mo_7O_{24}{\cdot}4H_2O$) was dissolved in 5 mL double distilled water (DDwater) with rapid and continuous stirring at room temperature. Subsequently, 0.19 g of NaH_2PO_4 dissolved in 5 mL DDwater was rapidly added. Then, 2 mL saturated L-ascorbic acid was slowly added dropwise into the solution. After 15 min, the POM was precipitated by adding 80 mL of ethanol and centrifuging at 11000 r/min for 15 min. The centrifuge was repeated 3 times. The obtained POM was dried in a vacuum dryer for 24 h to remove the ethanol completely. The products were redispersed in 10 mL PBS for further use.

Preparation and characterization of CDN–POM hydrogels.

40 mg smDNA and 2 mg POM were firstly dissolved in 1 mL of DD water at 100°C for 5 min. Then 0.1 mg PLL and 0.3 mg CDN were rapidly added. The complete gelation was achieved by cooling the heated DNA solution to room temperature, and kept for 12 h.

Scanning Electron Microscopy (SEM)

Morphology observation was performed by scanning electron microscopy (SEM, Phenom Pure) at 10 kV. Samples were mounted onto the specimen stubs by means of a conductive double-sided adhesive tape and sputtered with gold for 30 seconds.

Photothermal Conversion Performance of CDN–POM hydrogels.

The photothermal conversion ability of CDN–POM hydrogel was investigated by monitoring the temperature of 200 μL CDN–POM hydrogels (0.2% POM) under NIR laser irradiation. The temperature change of the CDN–POM hydrogels under NIR light irradiation was recorded by an IR thermal camera (Hikmicro). In addition, four NIR laser on/ off cycles were further carried out to evaluate the photothermal stability of the CDN–POM hydrogels.

ROS Scavenging Activities.

For H_2O_2 scavenging evaluation, 0, 100, 200, 300 and 400 μg/mL of POM were incubated with gradient concentrations of H2O2, and the related UV − vis-NIR spectra of the mixture were recorded. Following 30 min incubation with DCFH-DA at 37 ◦C, the cells were washed three times in the dark with PBS. Subsequently, the images were photographed using a fluorescence microscope (Olympus, Japan).

Cytotoxicity Evaluation.

Photothermal cell-killing efficiency of POM toward 4T1 breast cancer cells under NIR laser irradiation was then investigated by standard live/dead cell staining (Calcein-AM with green fluorescence for live cells and propidium iodide with red fluorescence for dead cells).

In vivo tumor retention assay by photoacoustic performance

All in vivo animal experimental procedures were approved by the Institutional Animal Care and Use Committee of the Fifth Affiliated Hospital of Sun Yat-sen University. Animal experiments were performed using female mice (Balb/c) at 4 weeks old (20 g body weight). Approximately 1×10^6 4T1 cells were subcutaneously inoculated on the right leg of mice and allowed to grow for 2 weeks, and typically, a solid tumor formed during this period. To analyze retention within the tumor, the tumor was injected with 100 μL CDN–POM hydrogels (0.2 w% POM) and POM (2000 ppm) (n = 3). All samples were simultaneously analyzed with a multispectral photoacoustic tomography (MSOT) system (Neuherberg, Germany) and an ultrasound research scanner (Redmond, WA, USA) for imaging at 870 nm excitation.

In Vivo Antitumor Study.

Female BALB/c nude mice-bearing 4T1 tumors with a volume of about 100 mm^3 were randomly divided into 5 groups (n = 5). The five groups were referred as (1) Subcutaneous injection of 100 μL PBS with 808 nm laser irradiation (Group 1: PBS + NIR.); (2) Subcutaneous injection of 100 μL POM solution with 808 nm laser irradiation (Group 2: POM + NIR); (3) Subcutaneous injection of 100 μL CDN hydrogels with 808 nm laser irradiation (Group 3: CDN hydrogels + laser); (4) Subcutaneous injection of 100 μL CDN–POM hydrogels (Group 4: CDN–POM hydrogels); (5) Subcutaneous injection of 100 μL CDN–POM hydrogels (0.2 w% POM) with 808 nm laser irradiation (Group 5:CDN–POM hydrogels + NIR). All the subcutaneous injection was conducted surround the tumors. At the tumor location, 808 nm laser irradiation with a power density of 1 W/cm^2 was used for 3 min. The total observation time was set for 21 days, and the tumor volume and body weight were recorded every 1 day. Vernier caliper was used to measure the

length (A) and width (B) of the tumors. The tumor volume was calculated as the formula: A*B*B/2. The current tumor size (V) divided by original tumor volume (V_0) to obtain relative tumor volume (V/V_0).

Histological Analysis

All the mice got sacrificed and dissected after observation for 21 days. Then the mice were euthanized, and fresh portions of the tissues or tumors site from each mouse were harvested rapidly. The organ (heart, liver, spleen, lung, and kidney) or tumor sections were cut into 5-μm thickness and mounted on the glass slides. The hematoxylin and eosin (H&E) staining were performed with protocols as described in the literature. The photographs of stained sections were taken by using an optical microscope (Nikon, Japan).

Immunohistochemistry

All the mice got sacrificed and dissected after observation for 7 days. For immunohistochemistry, the endogenous peroxidase was neutralized with 1% H_2O_2, followed by specific protein blockers; the slices were incubated with antibodies against TNF-α, IL-6, and IL-β at 4°C overnight, followed by incubating with HRP-conjugated anti-rabbit antibody for 60 min. The sections were visualized with diaminobenzidine (DAB) and counterstained with hematoxylin.

Statistical analysis

Quantitative data were presented as mean ± standard deviation. Significant differences between groups were indicated by *p<0.05, **p<0.01 and ***p<0.001.

Declarations

Author contributions

Hailong Jiang, Ke Zhang and Hong Shan conceived, designed and supervised the study. Hailong Jiang performed preparation and characterization of the hydrogels, cellular experiments and biodistribution, Die Liu, Hailong Jiang and Ke Zhang performed the histology, flow cytometry and analyzed the data. Jianing Wang, Jingchao Li, Xinrui Pang, Hong Shan, Ke Zhang and Hailong Jiang wrote and revised the paper. All authors discussed and approved the contents of the manuscript.

Funding

This work was financially supported by the National Natural Science Foundation of China Major Research Program on Molecular Function Visualization for Tumor Evolutionary Diagnosis and Treatment (92259204) and the National Natural Science Foundation of China (82102164).

Data availability

The datasets generated during and/or analyzed during the current study are available from the corresponding authors on reasonable request.

Competing interests

The authors have no relevant financial or non-financial interests to disclose.

Ethics approval

This study was performed in line with the principles of the Declaration of Helsinki. Approval was granted by the Ethics Committee of the Fifth Affiliated Hospital of Sun Yat-Sen University (No. 00329).

References

1. Xu Y, Gong M, Wang Y, Yang Y, Liu S, Zeng Q. Global trends and forecasts of breast cancer incidence and deaths. Sci Data. 2023;10(1):334.
2. Hamilton JB, Abiri AN, Nicolas CA, Gyan K, Chandler RD, Worthy VC, Grant EJ. African American Women Breast Cancer Survivors: Coping with the COVID-19 Pandemic. J cancer education: official J Am Association Cancer Educ. 2023;38(5):1539–47.
3. Suwankhong D, Liamputtong P, Boonrod T, Simla W, Khunpol S, Thanapop S. Breast Cancer and Screening Prevention Programmes: Perceptions of Women in a Multicultural Community in Southern Thailand. Int J Environ Res Public Health 20(6) (2023).
4. Hanna S, Lo SN, Saw RP. Surgical excision margins in primary cutaneous melanoma: A systematic review and meta-analysis. Eur J Surg oncology: J Eur Soc Surg Oncol Br Association Surg Oncol. 2021;47(7):1558–74.
5. Zhu M, Yang X, You J, Zheng L, Yi C, Huang Y. Nanobiotechnology-mediated radioimmunotherapy treatment for triple-negative breast cancer. MedComm – Biomaterials Appl 2(1) (2023).
6. Subhan MA, Parveen F, Shah H, Yalamarty SSK, Ataide JA, Torchilin VP. Recent Advances with Precision Medicine Treatment for Breast Cancer including Triple-Negative Sub-Type. Cancers 15(8) (2023).
7. Chupradit S, Widjaja G, Radhi Majeed B, Kuznetsova M, Ansari MJ, Suksatan W, Turki Jalil A. Ghazi Esfahani, Recent advances in cold atmospheric plasma (CAP) for breast cancer therapy. Cell Biol Int. 2023;47(2):327–40.
8. Fang Y, Huang S, Gong X, King JA, Wang Y, Zhang J, Yang X, Wang Q, Zhang Y, Zhai G, Ye L. Salt sensitive purely zwitterionic physical hydrogel for prevention of postoperative tissue adhesion. Acta Biomater. 2023;158:239–51.
9. Li Z, Yang L, Zhang D, Wang W, Huang Q, Liu Q, Shi K, Yu Y, Gao N, Chen H, Jiang S, Xie Z, Zeng X. Mussel-inspired plug-and-play hydrogel glue for postoperative tumor recurrence and wound infection inhibition. J colloid interface Sci 650(Pt B) (2023) 1907–17.

10. Zhang P, Cui Y, Wang Y. Designing temporal- and spatial-control multifunctional nanoformulations for synergistic photodynamic–enhanced tumour immunotherapy. Nano Today. 2023;49:101816.
11. Xiong Y, Rao Y, Hu J, Luo Z, Chen C. Nanoparticle-Based Photothermal Therapy for Breast Cancer Noninvasive Treatment, Advanced materials (2023) e2305140.
12. Nag S, Mitra O, Tripathi G, Adur I, Mohanto S, Nama M, Samanta S, Gowda BHJ, Subramaniyan V, Sundararajan V, Kumarasamy V. Nanomaterials-assisted photothermal therapy for breast cancer: State-of-the-art advances and future perspectives. Photodiagn Photodyn Ther. 2024;45:103959.
13. Marchi S, Guilbaud E, Tait SWG, Yamazaki T, Galluzzi L. Mitochondrial control of inflammation, Nature reviews. Immunology. 2023;23(3):159–73.
14. Chen Z, Han F, Du Y, Shi H, Zhou W. Hypoxic microenvironment in cancer: molecular mechanisms and therapeutic interventions. Signal Transduct Target therapy. 2023;8(1):70.
15. Guan H, Zou P, Lin R, Xiao L, Fang Z, Chen J, Lin T, Wang Y, Peng Y, Zhong T, Zhang B, Lang J, Zhang Y, Xing L, Chen M, Xue X. Implantable self-powered therapeutic pellet for wireless photodynamic/sonodynamic hybrid therapy of cancer recurrence inhibition and tumor regression. Nano Energy. 2023;105:108002.
16. Kiaie SH, Salehi-Shadkami H, Sanaei MJ, Azizi M, Shokrollahi Barough M, Nasr MS, Sheibani M. Nano-immunotherapy: overcoming delivery challenge of immune checkpoint therapy. J Nanobiotechnol. 2023;21(1):339.
17. Shi G, Jiang H, Yang F, Lin Z, Li M, Guo J, Liao X, Lin Y, Cai X, Li D. NIR-responsive molybdenum (Mo)-based nanoclusters enhance ROS scavenging for osteoarthritis therapy. Pharmacol Res. 2023;192:106768.
18. Yang F, Chen Y, Xiao Y, Jiang H, Jiang Z, Yang M, Li M, Su Y, Yan Z, Lin Y. pH-sensitive molybdenum (Mo)-based polyoxometalate nanoclusters have therapeutic efficacy in inflammatory bowel disease by counteracting ferroptosis. Pharmacol Res. 2023;188:106645.
19. Xue R, Liu Y-S, Wang M-Y, Guo H, Yang W, Yang G-Y. Combination of covalent organic frameworks (COFs) and polyoxometalates (POMs): the preparation strategy and potential application of COF–POM hybrids, Materials Horizons (2023).
20. Liu J, Huang M, Zhang X, Hua Z, Feng Z, Dong Y, Sun T, Sun X, Chen C. Polyoxometalate nanomaterials for enhanced reactive oxygen species theranostics. Coord Chem Rev. 2022;472:214785.
21. Zhou J, Zhao W, Miao Z, Wang J, Ma Y, Wu H, Sun T, Qian H, Zha Z. Folin-Ciocalteu Assay Inspired Polyoxometalate Nanoclusters as a Renal Clearable Agent for Non-Inflammatory Photothermal Cancer Therapy. ACS Nano. 2020;14(2):2126–36.
22. Tao Z, Wang J, Wu H, Hu J, Li L, Zhou Y, Zheng Q, Zha L, Zha Z. Renal Clearable Mo-Based Polyoxometalate Nanoclusters: A Promising Radioprotectant against Ionizing Irradiation. ACS Appl Mater Interfaces. 2023;15(9):11474–84.
23. Perciani CT, Liu LY, Wood L, MacParland SA. Enhancing Immunity with Nanomedicine: Employing Nanoparticles to Harness the Immune System. ACS Nano. 2021;15(1):7–20.

24. Krejcik J, Barnkob MB, Nyvold CG, Larsen TS, Barington T, Abildgaard N. Harnessing the Immune System to Fight Multiple Myeloma. Cancers. 2021;13(18):4546.
25. Luo W-W, Tong Z, Cao P, Wang F-B, Liu Y, Zheng Z-Q, Wang S-Y, Li S, Wang Y-Y. Transcription-independent regulation of STING activation and innate immune responses by IRF8 in monocytes. Nat Commun 13(1) (2022).
26. Wang X, Yang C, Wang X, Miao J, Chen W, Zhou Y, Xu Y, An Y, Cheng A, Ye W, Chen M, Song D, Yuan X, Wang J, Qian P, Wu AR, Zhang Z-Y, Liu K. Driving axon regeneration by orchestrating neuronal and non-neuronal innate immune responses via the IFNγ-cGAS-STING axis. Neuron. 2023;111(2):236–e2557.
27. Ji Y, Luo Y, Wu Y, Sun Y, Zhao L, Xue Z, Sun M, Wei X, He Z, Wu SA, Lin LL, Lu Y, Chang L, Chen F, Chen S, Qian W, Xu X, Chen S, Pan D, Zhou Z, Xia S, Hu C-CA, Liang T, Qi L. SEL1L–HRD1 endoplasmic reticulum-associated degradation controls STING-mediated innate immunity by limiting the size of the activable STING pool. Nat Cell Biol. 2023;25(5):726–39.
28. Tan J, Wang M, Ding B, Lin J. Advanced nanomaterials targeting activation of STING for enhanced cancer immunotherapy. Coord Chem Rev. 2023;493:215316.
29. Zhang J, Yu S, Peng Q, Wang P, Fang L. Emerging mechanisms and implications of cGAS-STING signaling in cancer immunotherapy strategies. Cancer Biology Med. 2024;21(1):45.
30. Hong Z, Mei J, Li C, Bai G, Maimaiti M, Hu H, Yu W, Sun L, Zhang L, Cheng D. STING inhibitors target the cyclic dinucleotide binding pocket, Proceedings of the National Academy of Sciences 118(24) (2021) e2105465118.
31. Leach DG, Dharmaraj N, Piotrowski SL, Lopez-Silva TL, Lei YL, Sikora AG, Young S, Hartgerink JD. STINGel: Controlled release of a cyclic dinucleotide for enhanced cancer immunotherapy, Biomaterials 163 (2018) 67–75.
32. AduroBiotech N. Study of the Safety and Efficacy of MIW815 (ADU-S100) in Patients With Advanced. Metastatic Solid Tumors or Lymphomas 2(5) (2016).
33. Corrales L, Glickman LH, McWhirter SM, Kanne DB, Sivick KE, Katibah GE, Woo S-R, Lemmens E, Banda T, Leong JJ, Metchette K, Dubensky TW, Gajewski TF. Direct Activation of STING in the Tumor Microenvironment Leads to Potent and Systemic Tumor Regression and Immunity. Cell Rep. 2015;11(7):1018–30.
34. Chen X, Meng F, Xu Y, Li T, Chen X, Wang H. Chemically programmed STING-activating nano-liposomal vesicles improve anticancer immunity. Nat Commun. 2023;14(1):4584.
35. Xu C, Dobson HE, Yu M, Gong W, Sun X, Park KS, Kennedy A, Zhou X, Xu J, Xu Y, Tai AW, Lei YL, Moon JJ. STING agonist-loaded mesoporous manganese-silica nanoparticles for vaccine applications. J controlled release: official J Controlled Release Soc. 2023;357:84–93.
36. Liu B, Sun J, Zhu J, Li B, Ma C, Gu X, Liu K, Zhang H, Wang F, Su J, Yang Y. Injectable and NIR-Responsive DNA-Inorganic Hybrid Hydrogels with Outstanding Photothermal Therapy. Adv Mater. 2020;32(39):e2004460.

Figures

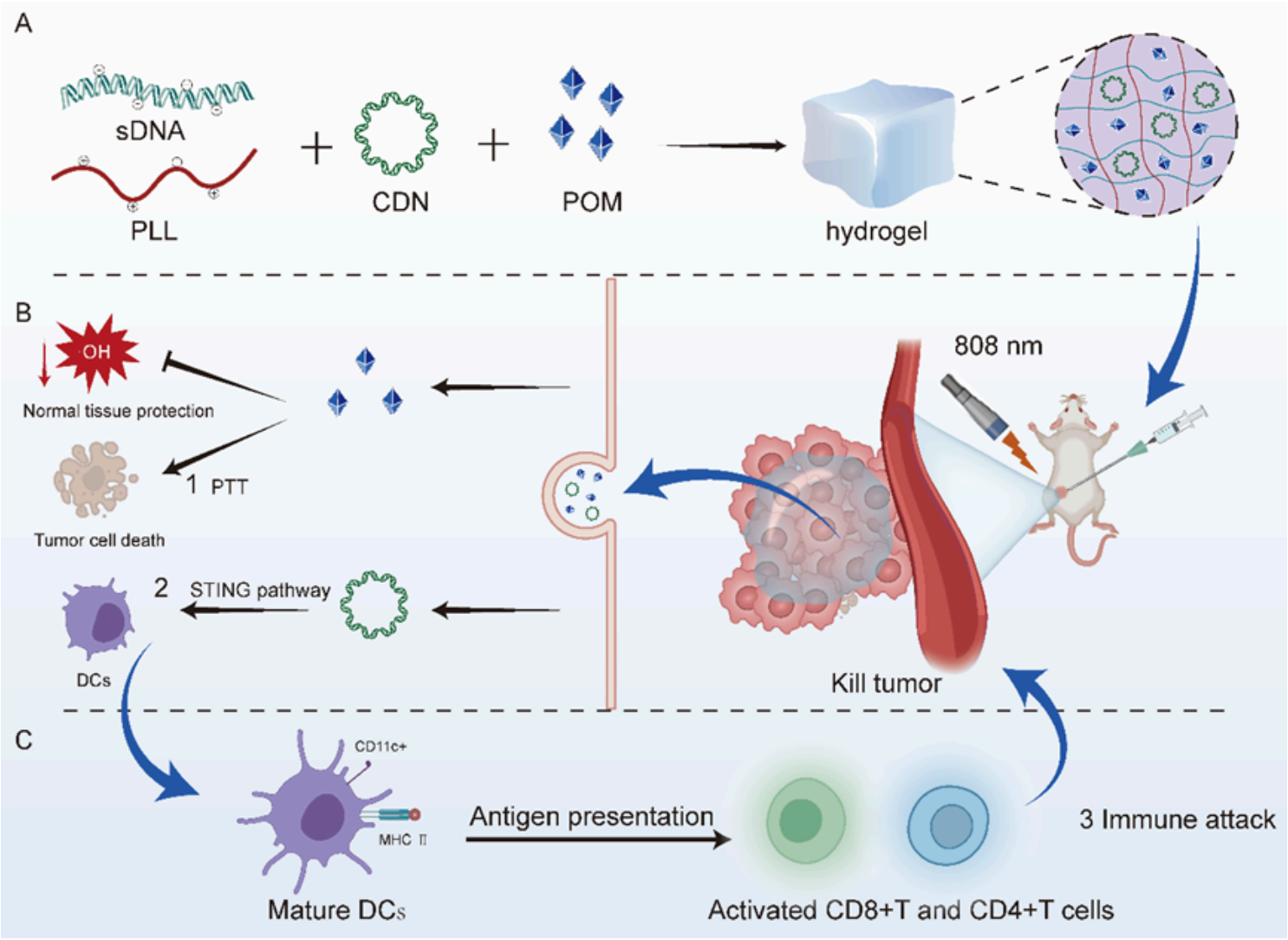

Figure 1

Schematic illustration of the combinatorial non-inflammatory photothermal therapy and immunotherapy against breast tumor induced by CDN-POM hydrogels.

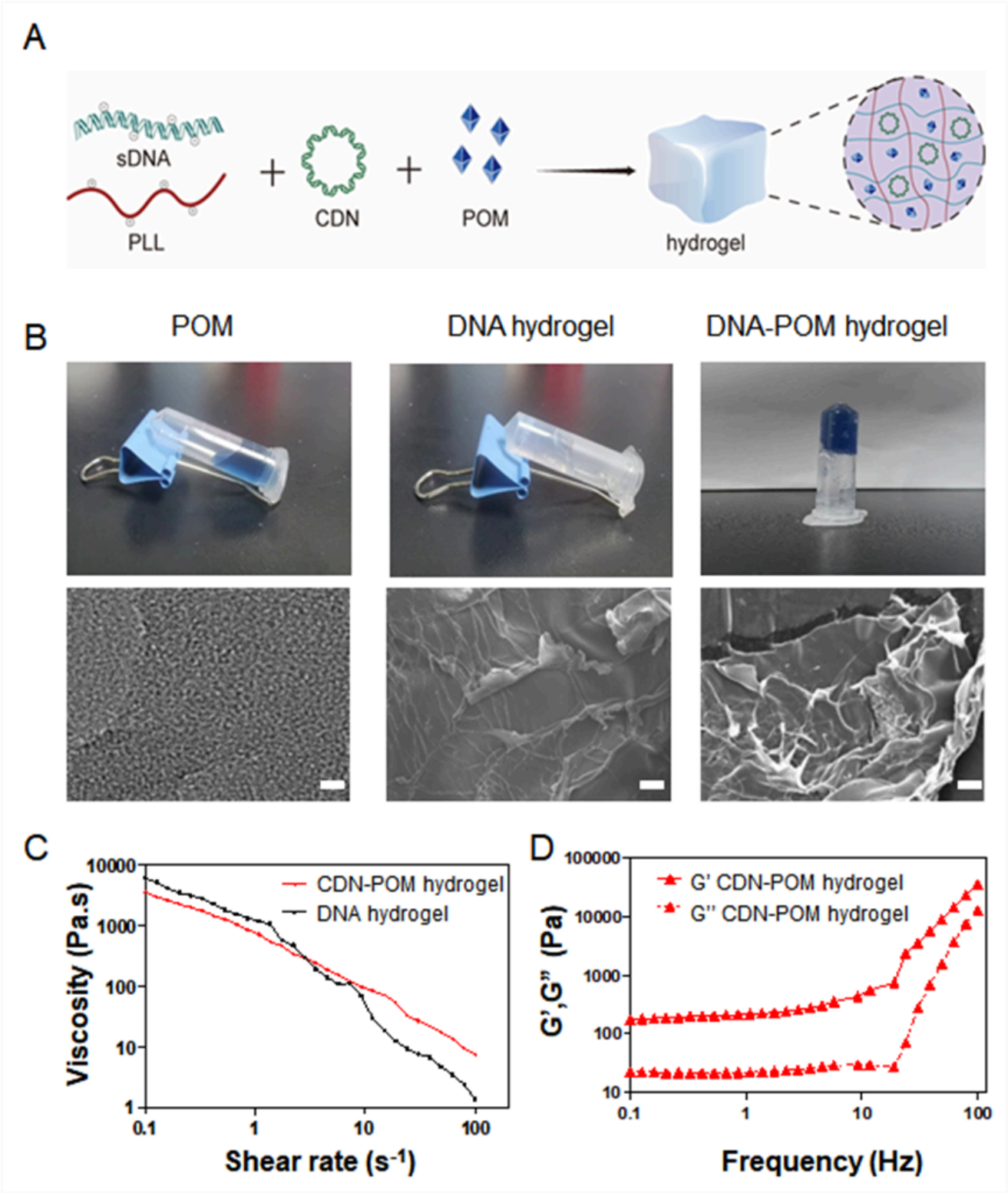

Figure 2

Preparation and characterizations of the CDN-POM hydrogel. The CDN-POM hydrogels were formed by electrostatic complexation of salmon DNA, POM, CDN and PLL. The electrostatic interactions between negatively charged smDNA, POM, CDN and positively charged PLL facilitate the formation of crosslink networks and further enhance the hardness of hydrogel. Scale bar: 1 cm. B) Scanning electron microscopy (SEM) image of the CDN-POM hydrogel. Scale bar: 30 μm. C) Viscosity measurement of the

CDN-POM hydrogel. D) Dependence of storage (G') and loss (G") moduli on frequency for the CDN-POM hydrogel, indicating the viscoelastic property.

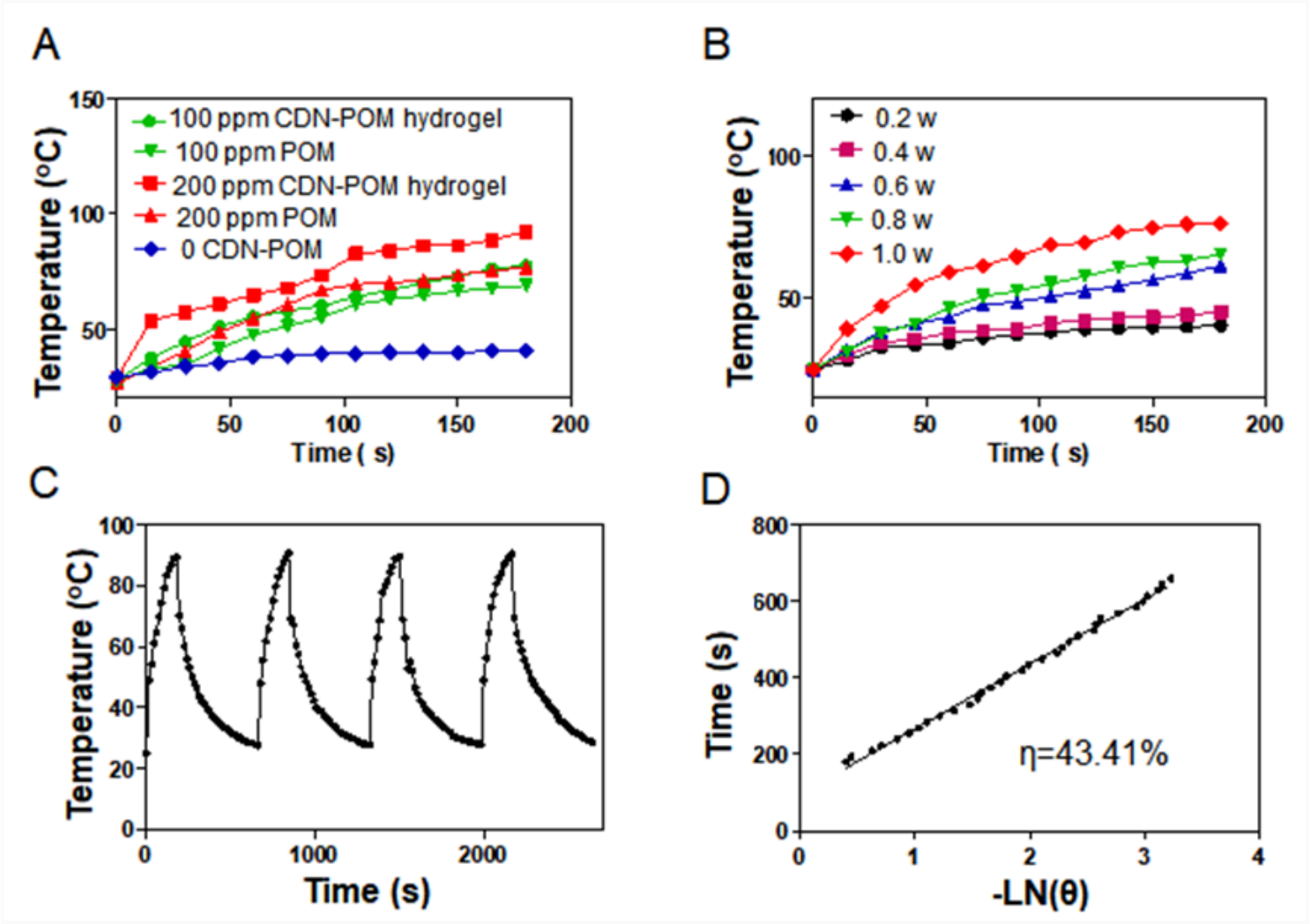

Figure 3

Photothermal conversion performance of the CDN-POM hydrogel. A) Time-dependent temperature evolution of the CDN-POM hydrogel under NIR light irradiation. pristine DNA, and POM as the control (1 W cm^{-2}). B) Heating curves of 0.2 wt% CDN-POM hydrogel under 808 nm laser irradiation with different power densities. C) Heating and cooling curves of the CDN-POM hydrogel (0.2 wt% POM) under 808 nm laser irradiation (1 W/cm^2). (D) Time constant for heat transfer calculated *via* the cooling portion of (C). The photo-thermal conversion efficiency (η) was calculated as follows: η=hS (T_{max}, POM-T_{max}, solvent)/I(1-10^{-A808}); t=-t_sLnθ;θ=(T-T_{sur})/(T_{max},NPs-T_{surr}); hS=mdCd/s. The photo-thermal conversion efficiencies of POM and CDN-POM hydrogel were 32.3% and 43.41% respectively.

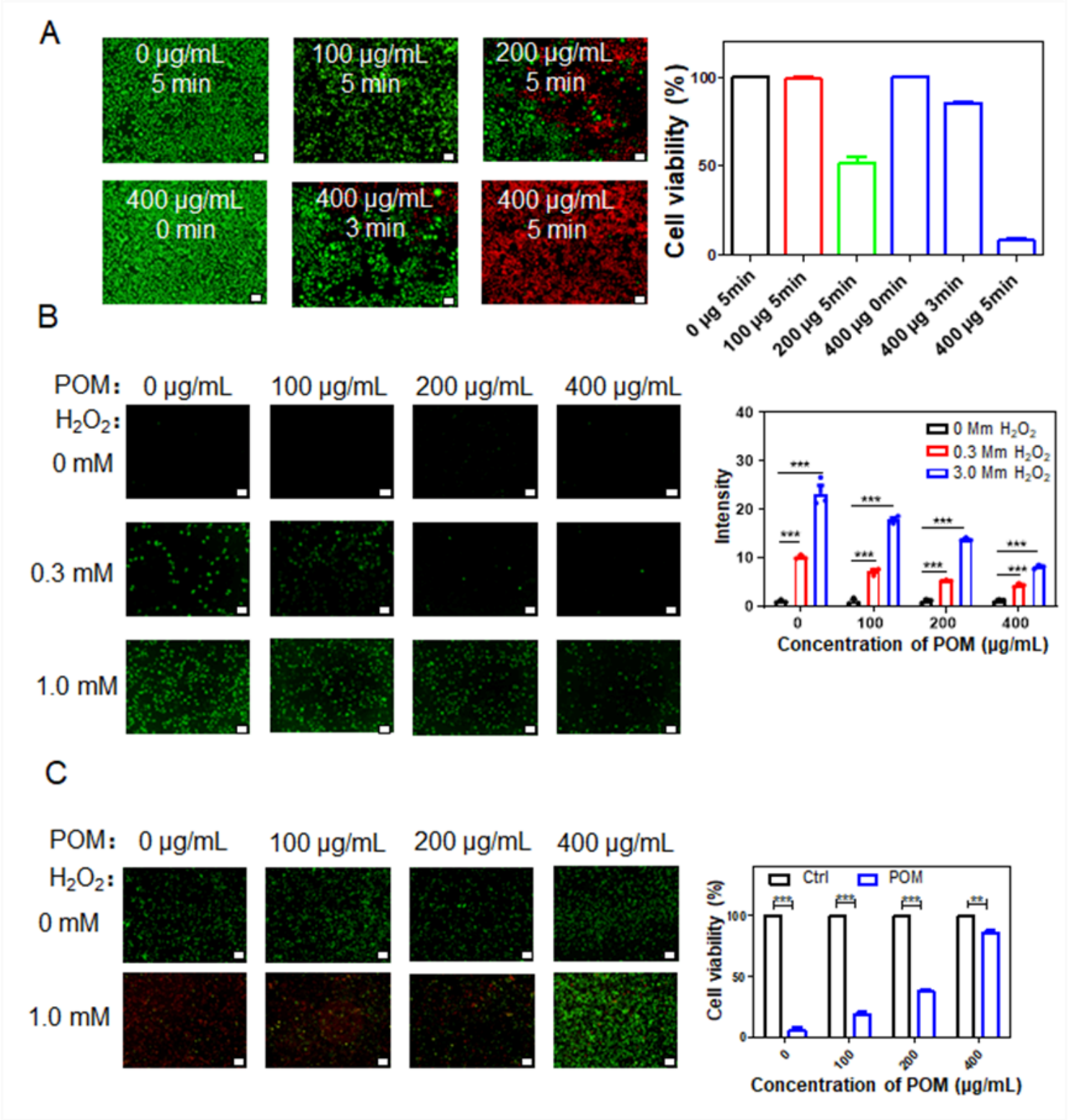

Figure 4

Characterization of in vitro cell killing efficiency and ROS scavenging activities of POM. A) Live/dead assay for evaluation of localized photothermal ablation. (B) relative percent ROS levels in 293T under different treatments. (C) Typical live/dead cell staining assay. Scale bar: 50 μm.

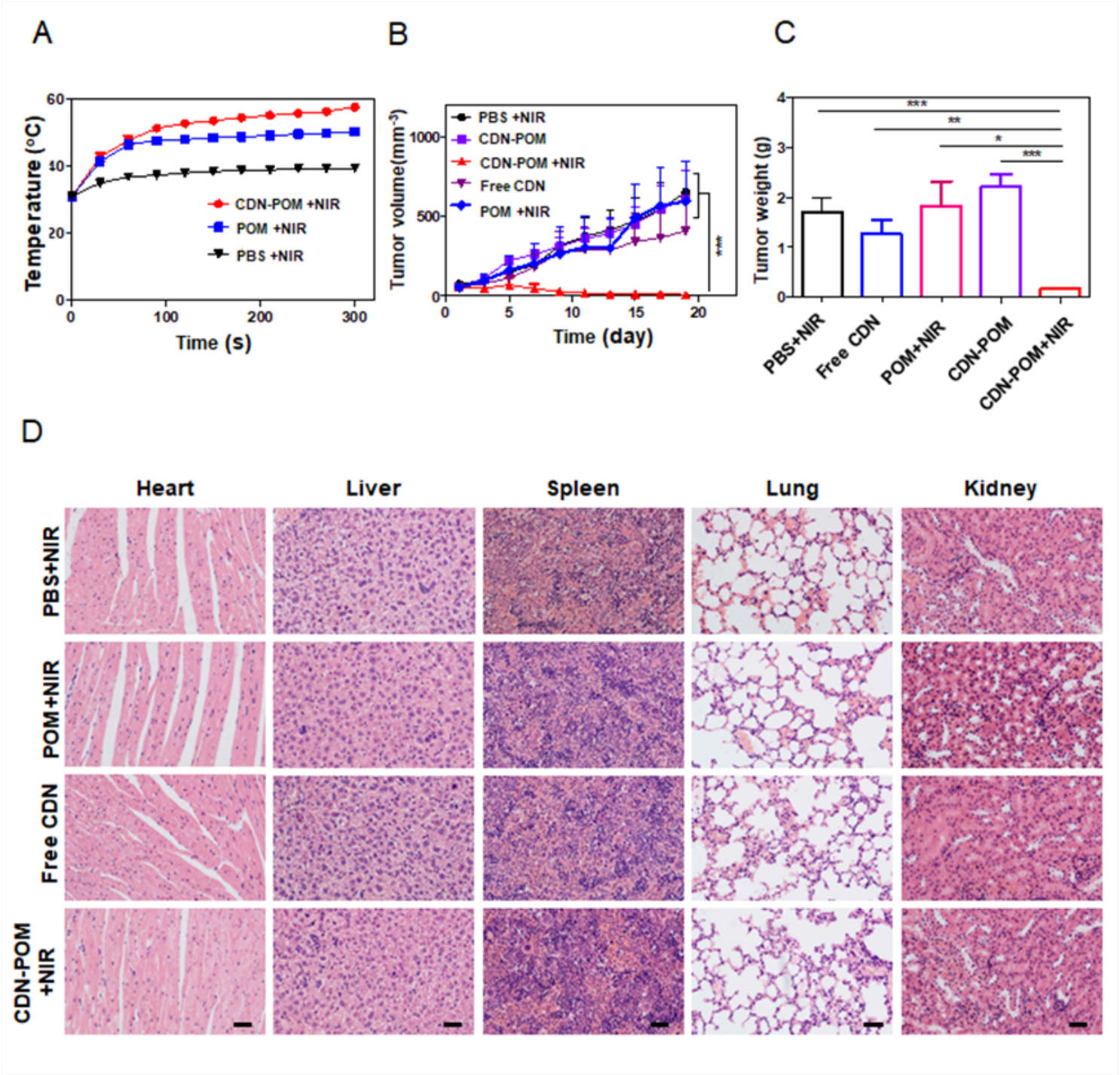

Figure 5

A) Time-dependent temperature evolution of the CDN-POM hydrogel under NIR light irradiation. PBS, and POM as the control (1 W/cm^2). B) Tumor volume monitoring curves (*p < 0.05, **p< 0.01). C) The weights of tumors excised from different groups after the final administration (n = 5). D) H&E staining of tumor slices after various treatments. Scale bar: 100 μm.

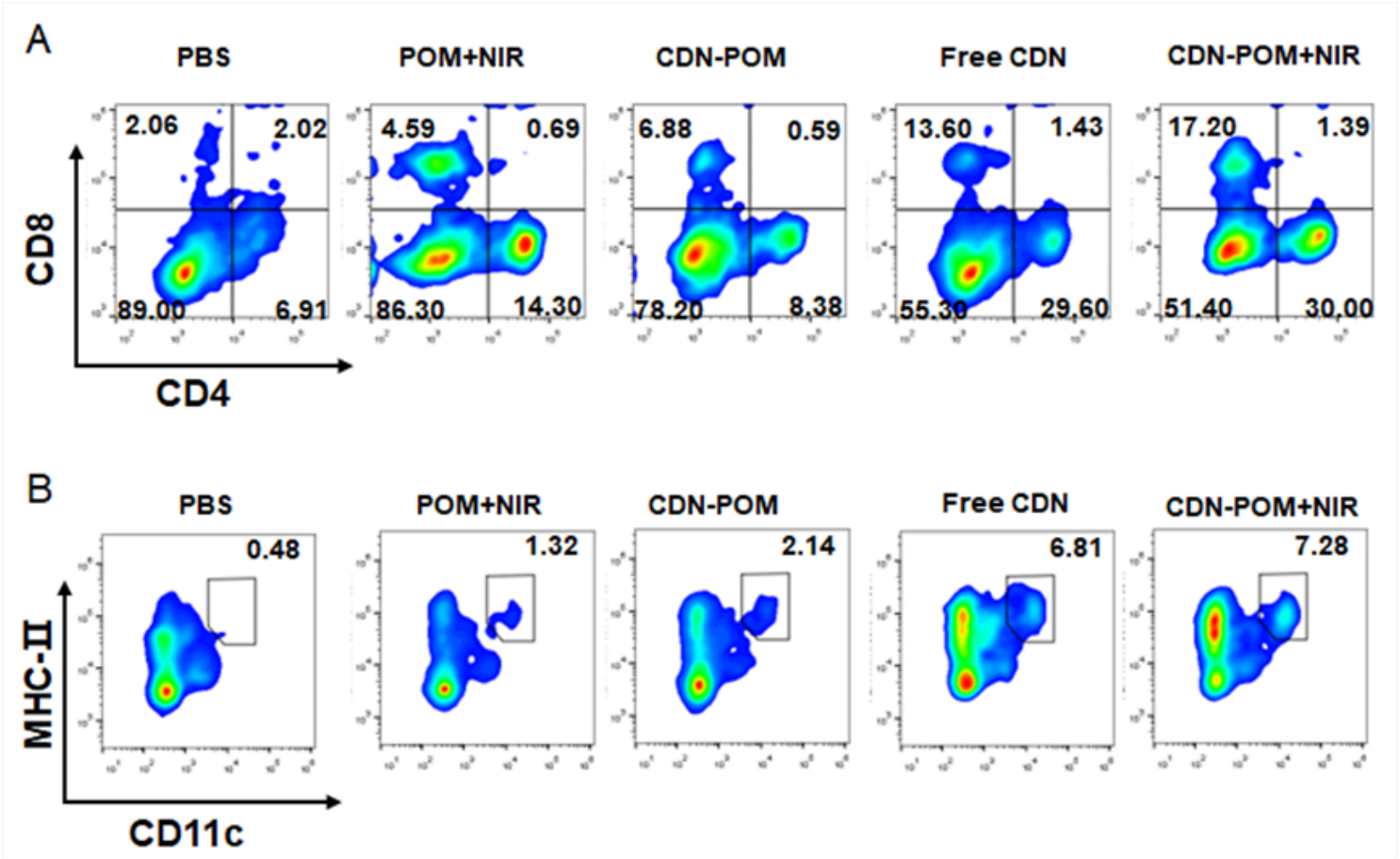

Figure 6

Evaluation of Cellular Immunity. A) Flow cytometry analysis of positive $CD4^+$ T cells or $CD8^+$ T cells. B) Flow cytometry analysis of MHC- II or CD11c cells in MDSCs.

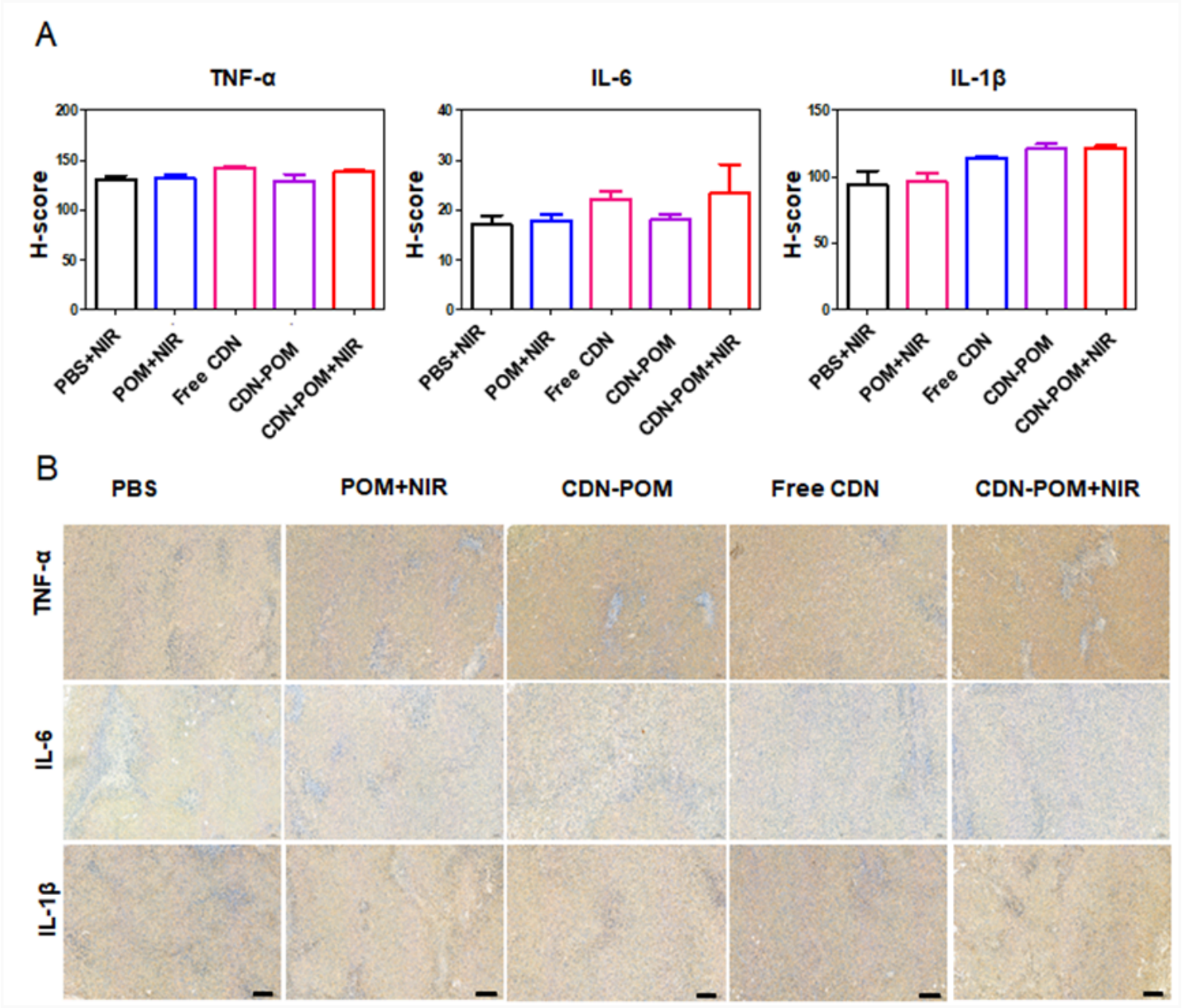

Figure 7

(a) Determination of the levels of inflammation-related cytokines including TNF-α, IL-6, and IL-β in Balb/c mice (n = 3) after various treatments as indicated (*p < 0.05, **p < 0.01). (b) Typical immunohistochemical staining images of related inflammatory cytokines. Scale bar: 100 μm.

Supplementary Files

This is a list of supplementary files associated with this preprint. Click to download.

- SI.docx